Fully differential cross sections for single ionizing 1-Mev p+He collisions at small momentum transfer: Beyond the first Born approximation

O. Chuluunbaatar[1,2], S. A. Zaytsev[3], K. A. Kouzakov[4],

A. Galstyan[5], V. L. Shablov[6], and Yu. V. Popov[7,1*]

[1]*Joint Institute for Nuclear Research,*

Dubna, Moscow region 141980, Russia

[2]*Institute of Mathematics, National University of Mongolia, UlaanBaatar, Mongolia*

[3]*Department of Physics, Pacific State University,*

Tikhookeanskaya 136, Khabarovsk 680035, Russia

[4]*Department of Nuclear Physics and Quantum Theory of Collisions,*

Faculty of Physics, Lomonosov Moscow State University, Moscow 119991, Russia

[5]*Institute of Condensed Matter and Nanosciences,*

Université Catholique de Louvain, 2 chemin du cyclotron,

Box L7.01.07, B-1348 Louvain-la-Neuve, Belgium

[6]*Obninsk Institute for Nuclear Power Engineering of the*

National Research Nuclear University MEPhI, Russia and

[7]*Skobeltsyn Institute of Nuclear Physics,*

Lomonosov Moscow State University, Moscow 119991, Russia

Abstract

We present calculations of the electron angular distributions in the single ionization of helium by 1-MeV proton impact at momentum transfer of 0.75 a.u. and ejected-electron energy of 6.5 eV. The results using the first and second Born approximations and the 3C model with different trial helium functions are compared to the experimental data. A good agreement between theory and experiment is found in the case of the 3C final state and a strongly correlated helium wave function. The electron-electron correlations in the He atom are found to influence the ratio of the binary and recoil peak intensities.

PACS numbers: 34.50.Fa, 52.20.Hv

---

* popov@srd.sinp.msu.ru

I. INTRODUCTION

Single ionization of atomic targets by fast ions in a perturbative regime has been attracting much interest from experimentalists and theorists in recent years. This is largely due to a remarkable progress of the technique known as cold target recoil ion momentum spectroscopy (COLTRIMS) [1–3]. COLTRIMS is a reaction microscope that allows one to measure in coincidence with the residual ion three-dimensional angular distributions of electrons emitted in the ionizing ion-atom collisions at given values of energy and momentum transfer with unprecedented precision. Thus, different theoretical approaches, in particular, those based on the plane wave first Born approximation (PWFBA), can be very robustly tested by comparing their predictions for the fully differential cross sections (FDCS) with the COLTRIMS data.

When comparing theory and experiment, the one of the most interesting angular regions appears to be the one separating the binary and recoil peaks, where a distinct node is generally predicted by perturbation treatments. It is the region where marked discrepancies between theory and experiment were found in the case of singly ionizing 100-MeV/u C^{6+}+He collisions at momentum transfer of 0.75 a.u. [4]. The node in the measured electron emission pattern was much less pronounced than that anticipated by theory. This finding was particularly surprising given the fact that the measurements were carried out under kinematical conditions which are believed to be perfectly suitable for applicability of perturbative approaches: (i) $|Z_p|/v_p = 0.1$ a.u., where Z_p and v_p are the projectile charge and velocity, respectively, and (ii) small energy- and momentum-transfer values. Further discussions involved various attempts to explain the source of the discrepancies in the nodal structure, ranging from higher-order [4–8] and non-perturbative mechanisms [7, 9–12] to experimental uncertainties [8, 13] and so-called projectile coherence effects [14]. Though the explanation due to experimental uncertainties alone was refuted in [15], the very recent 1-MeV p+He experiment at momentum transfer of 0.75 a.u. [16], which has been performed with the highest momentum resolution ever achieved in such ionizing ion-atom collisions, has exhibited a well-pronounced nodal structure.

It should be noted that the analysis of the data of that experiment has not revealed clear footprints of the projectile coherence effects. At the same time, according to the criteria formulated in Wang et al. [14], the calculated transverse coherence lengths for a rectangularly

collimated projectile beam in the discussed experiment were in the intermediate regime, i.e. not large enough to yield a coherent beam and not sufficiently small to yield an incoherent beam. This means that the problem of the projectile coherence can still be claimed as not completely resolved (see, for instance, the recent work [17]). The most recent theoretical analyses and discussions devoted to this problem one can find in Refs. [18–20] and references therein.

For shedding light onto the origin of the disagreement between theory and experiment one must also analyse the role of theoretical uncertainties, which are due to inaccuracy of theoretical models employed for calculations of FDCS. These uncertainties arise from approximations involved in the treatment both of the collision mechanism and of the initial and final states of the target. Therefore, apart from delivering details of experiment that determine momentum resolution and projectile-coherence effects, the purpose of this work is to present theoretical calculations of FDCS using different models of the initial and final helium states as well as different models of the collision mechanism. Currently there are two main theoretical approaches to ionization of a quantum target by impact of a proton (positive ion). These are the continuum distorted wave-eikonal initial state (CDW-EIS) method in the semiclassical and fully quantum formulations respectively. In the semiclassical approach, one treats the proton as a classical particle moving along a straight-line trajectory with an impact parameter ρ and velocity v_p, which induces time-dependent perturbation of the quantum target. The time-dependent Schrödinger equation for the target is solved with the appropriate boundary condition at $t \to -\infty$. In the quantum approach, one solves a stationary quantum scattering problem for all particles involved in the ionization reaction. An example of semiclassical calculations for the kinematical domain discussed in the present work can be found in [21].

To the best of our knowledge, for the first time the stationary formulation of the CDW-EIS method was given in Refs. [22, 23]. It was further developed in later works (see, for instance, Refs. [9, 24]). Though some of them dealt with charge-transfer reactions, the quantum CDW-EIS method was elaborated in these works rather fully. The semiclassical CDW-EIS method was formulated for the first time, to the best of our knowledge, in Ref. [25] (strictly speaking, J. Cheshire formulated a CDW-CDW model). Later it was developed in Refs. [26, 27], which are mainly cited by the authors of more recent works (see, for instance, those by the group of Rivarola *et al.* [28, 29]). Both formulations, along with their relation

to each other within a rigorous mathematical approach, are discussed in the well-known review articles [30, 31].

Besides the CDW-EIS method there are more traditional approaches in the literature, where in the exact post-form matrix element for the transition amplitude the full final-state wave function is replaced with its various approximations. It is believed that the closer the asymptotics of the approximate wave functions to the exact asymptotics at large distances between the particles the better such approximations work. In this regard, it is worth to mention the works of Madison *et al.* (see, for instance, Refs. [5, 10]). Clearly, all the above-mentioned methods and approaches are related to each other in one way or another, and they well explain discrepancies between PWFBA and experiment at high incident energy of a projectile (proton). It should be noted that very often they yield practically the same results in the most of kinematical regions of ionization reactions with MeV's protons.

The special case of the quantum CDW-EIS is the so-called 3C (or BBK) model [32]. In this model, three Coulomb continuum functions are employed for description of the final-state interactions. It should be noted that most of the matrix-element calculations are performed in real space using trial wave functions of the target that are rather simple. The latter is due to the complexity of the calculations (see, for instance, Ref. [33]).

In this work, we present calculations of FDCS beyond the PWFBA theory in order to explain the shift of the measured binary and recoil peaks in the scattering plane by few degrees towards the incident proton direction with respect to the PWFBA predictions [16]. For this purpose we examine the plane wave second Born approximation (PWSBA) and the well-known 3C (or BBK) model [32]. The calculations are performed in momentum space, what allows one to inspect different models of the helium ground state, including the strongly correlated ones. Three different ground-state wave functions of He are used in the calculations: (i) the loosely correlated Roothaan-Hartree-Fock function (RHF) [35], (ii) the trial wave function of Silverman-Platas-Matsen (SPM) [36] from the configuration interaction family, and (iii) a strongly correlated function (CF) [37] of the Bonham-Kohl type. For accurate comparisons with experiment, all theoretical values are convoluted with experimental uncertainties.

The paper is organized as follows. In Sec. II, we formulate different theoretical models and approximations for the considered process. Then, in Sec. III, we compare experimental and theoretical results. The conclusions are drawn in Sec. IV. Atomic units (a.u.), in which

$\hbar = e = m_e = 1$, are used throughout unless otherwise specified.

II. THEORY

In Ref. [16], we calculated FDCS for the discussed ionization reaction using the PWFBA. We designate the incident and final proton momenta by $\vec{p}_i$ and $\vec{p}_s$, respectively, the electron momentum by $\vec{k}_e$, the final ion momentum by $\vec{K}_{ion}$. In the experiment, the momentum transfer Q is relatively small, $Q = 0.75$ a.u., and the ejected-electron is $E_e = 6.5$ eV (0.24 a.u.). The momentum conservation law

$$\vec{Q} = \vec{p}_i - \vec{p}_s = \vec{k}_e + \vec{K}_{ion} \tag{1}$$

shows that the velocity of the residual ion $K_{ion}/(m_N + 1)$ is practically negligible (the mass of the He atom is $m_N \approx 4m_p = 7344.6$ a.u.), what allows us to choose the stationary He nucleus as a center of the laboratory coordinate system.

From the energy conservation law

$$E = \frac{p_i^2}{2m_p} + \varepsilon_0^{He} = \frac{(\vec{p}_i - \vec{Q})^2}{2m_p} + \varepsilon_0^{He^+} + \frac{k_e^2}{2} + \frac{K_{ion}^2}{2(m_N + 1)} \tag{2}$$

one obtains the z-component of the momentum transfer as $Q_z = (-\varepsilon_0^{He} + \varepsilon_0^{He^+} + E_e)/v_p = 0.18$ a.u. (the z axis is directed along the initial proton momentum $\vec{p}_i$). The transverse component is $Q_\perp \approx m_p v_p \theta_s = 0.73$ a.u. (θ_s is the scattering angle of the proton), with $v_p = p_i/m_p$ being the proton velocity. The He and He$^+$ kinetic energies, $Q^2/2m_p$ and $K_{ion}^2/2(m_N + 1)$, are neglected in Eq. (2).

The general expression for FDCS reads

$$\frac{d^3\sigma}{dE_e d\Omega_e d\Omega_s} = k_e \frac{m_p^2}{(2\pi)^5} |T_{fi}|^2. \tag{3}$$

This form is different from that in Ref. [5]. It is correct for small momentum transfers, when the velocity of the recoil ion is practically zero. In this case we can place the center of coordinates at the ion and use the proton mass m_p instead of the reduced mass $\mu_{pN} = m_p m_N/(m_p + m_N)$ [38].

The final state of the considered reaction contains three charged fragments: p, e and the He$^+$ ion. In general, the Dollard asymptotic conditions [34] should be taken into account.

6

Within the PWFBA these conditions are discarded. Below we consider a correlated 3C final-state wave function Φ_f [32] which satisfies these conditions.

As indicated in the introduction section, three initial trial helium wave functions Φ_0^{He} are employed: a weakly correlated Roothaan-Hartree-Fock (RHF) [35] function, $\varepsilon_0^{RHF} = -2.8617$ a.u., a simple Silverman-Platas-Matsen (SPM) function [36] of the configuration interaction family, $\varepsilon_0^{SPM} = -2.8952$ a.u., and a strongly correlated function (CF) [37] which explicitly depends on the r_{12} distance between electrons in helium, $\varepsilon_0^{CF} = -2.903724$ a.u.. The helium energy of last function is very close to the experimental value, $\varepsilon_0^{He} = -2.903724$ a.u..

General formulas for the 3C wave function

In this approximation, the matrix element has the following form (the electron identity is taken into account by the factor of $\sqrt{2}$):

$$T_{fi}^{3C} = \sqrt{2} \int d^3R d^3r_1 d^3r_2 \, e^{i\vec{R}\vec{p}_i} \Psi_f^{(-*)}(\vec{R}, \vec{r}_1, \vec{r}_2; \vec{p}_s, \vec{k}_e) \Phi_0^{He}(\vec{r}_1, \vec{r}_2)$$

$$\times \left[\frac{2}{R} - \frac{1}{|\vec{R} - \vec{r}_1|} - \frac{1}{|\vec{R} - \vec{r}_2|} \right], \tag{4}$$

where the final-state wave function is

$$\Psi_f^{-*}(\vec{R}, \vec{r}_1, \vec{r}_2) = e^{-i\vec{R}\vec{p}_s} \varphi_0^{He^+}(\vec{r}_2) \tilde{\phi}^{-*}(\vec{k}_e, \vec{r}_1; -1) \exp\left(\frac{\pi}{2|\vec{v}_p - \vec{k}_e|} \right) \Gamma\left(1 - i\frac{1}{|\vec{v}_p - \vec{k}_e|} \right)$$

$$\times {}_1F_1\left[i\frac{1}{|\vec{v}_p - \vec{k}_e|}, 1; i(|\vec{R} - \vec{r}_1||\vec{v}_p - \vec{k}_e| + (\vec{R} - \vec{r}_1) \cdot (\vec{v}_p - \vec{k}_e)) \right]$$

$$\times \exp\left(-\frac{\pi}{2v_p} \right) \Gamma\left(1 + i\frac{1}{v_p} \right) {}_1F_1\left[-i\frac{1}{v_p}, 1; i(Rp_r + \vec{R} \cdot \vec{p}_r) \right]. \tag{5}$$

This is the 3C (BBK) function. Here $\vec{r}_1$, $\vec{r}_2$, and $\vec{R}$ are the electron and proton positions with respect to the nucleus,

$$\vec{p}_r = [(4m_p + 1)\vec{p}_s - m_p \vec{K}_{ion}]/(5m_p + 1) \approx (4m_p/5)\vec{v}_p + (1/5)\vec{k}_e - \vec{Q},$$

and $m_p = 1836.15$ a.u. is the proton mass. Further, $\vec{p}_i = m_p \vec{v}_p$, $v_p = 6.35$ a.u.,

$$\tilde{\phi}^{-*}(\vec{q}, \vec{r}; Z) = e^{-\pi\xi/2} \Gamma(1 + i\xi) e^{-i\vec{q}\cdot\vec{r}} {}_1F_1(-i\xi, 1; iqr + i\vec{q} \cdot \vec{r})$$

is the Coulomb continuum function, with $\xi = Z/v_q$, where $Z = Z_j Z_k$ (Z_j and Z_k are charges of interacting particles). Finally, the ion ground state is

$$\varphi_0^{He^+}(\vec{r}_2) = \sqrt{\frac{8}{\pi}} \exp(-2r_2). \tag{6}$$

7

The PWFBA follows from Eq. (5) if one formally sets $1/v_p = 0$ and $1/|\vec{v}_p - \vec{k}_e| = 0$.

Let us explain our choice of the charges in the 3C wave function, especially in the Coulomb function $\tilde{\phi}^{-*}(\vec{k}_e, \vec{r}_1; -1)$, which describes an escape of the electron from the helium atom. The 3C function is basically asymptotic, providing the correct Dollard asymptotic behavior. If we would like to treat the motion of the escaping electron in the realistic potential, which is much more complex than a Coulomb potential, then we must deal with a full four-body problem inside the atomic target. This would bring about great difficulties from the viewpoint of numerical computations.

For numerical calculations on the basis of (4) it is convenient to perform its Fourier transformation that reduces significantly the number of integrations. The amplitude splits into the sum of three integrals, $T_{fi} = A_1 + A_2 + A_3$. We treat them separately and obtain

$$A_1 = 2\sqrt{2} \int \frac{d^3p}{(2\pi)^3} \; \phi^{-*}(\vec{v}_p - \vec{k}_e, \vec{p} + \vec{v}_p - \vec{k}_e; -1) I(\vec{p}_r, \vec{Q} + \vec{p}_r - \vec{p}; 1) G(\vec{k}_e, \vec{p}, 0), \qquad (7)$$

$$A_2 = -\sqrt{2} \int \frac{d^3p}{(2\pi)^3} \; I(\vec{v}_p - \vec{k}_e, \vec{p} + \vec{v}_p - \vec{k}_e; -1) \phi^{-*}(\vec{p}_r, \vec{Q} + \vec{p}_r - \vec{p}; 1) G(\vec{k}_e, \vec{p}, 0), \qquad (8)$$

$$A_3 = -4\pi\sqrt{2} \int \frac{d^3p_1}{(2\pi)^3} \frac{d^3p_2}{(2\pi)^3 p_2^2} \; \phi^{-*}(\vec{v}_p - \vec{k}_e, \vec{p}_1 + \vec{v}_p - \vec{k}_e; -1)$$
$$\times \; \phi^{-*}(\vec{p}_r, \vec{Q} + \vec{p}_r - \vec{p}_1 - \vec{p}_2; 1) G(\vec{k}_e, \vec{p}_1, \vec{p}_2). \qquad (9)$$

In $(7) \div (9)$ we have used the following notations:

$$I(\vec{q}, \vec{p}; Z) = \lim_{\lambda \to +0} \int \frac{d^3r}{r} e^{-\lambda r} \tilde{\phi}^{-*}(\vec{q}, \vec{r}; Z) e^{i\vec{p}\cdot\vec{r}} = \lim_{\lambda \to +0} 4\pi \; e^{-\pi\xi/2} \Gamma(1 + i\xi) \frac{[p^2 - (q + i\lambda)^2]^{i\xi}}{[(\vec{p} - \vec{q})^2 + \lambda^2]^{(1+i\xi)}}, \qquad (10)$$

$$\phi^{-*}(\vec{p}, \vec{q}; Z) = -\frac{\partial}{\partial\lambda} \; I(\vec{p}, \vec{q}; Z),$$

and

$$G(\vec{k}, \vec{q}_1, \vec{q}_2) = \int d^3r_1 d^3r_2 \; \tilde{\phi}^{-*}(\vec{k}, \vec{r}_1; -1) e^{i\vec{q}_1 \cdot \vec{r}_1} \varphi_0^{He^+}(\vec{r}_2) e^{i\vec{q}_2 \cdot \vec{r}_2} \Phi_0^{He}(\vec{r}_1, \vec{r}_2). \qquad (11)$$

For most of the He ground-state models the function $G(\vec{k}, \vec{q}_1, \vec{q}_2)$ is the analytical function or an integral of much lower dimension.

Some comments should be made about details of calculations. We investigated the behavior of the results of integration of $(7) \div (9)$ with a finite parameter λ. It was found that at $\lambda = 10^{-2} \div 10^{-4}$ we obtain very good stability of calculations and convergence. Results with $\lambda = 10^{-3}$ and $\lambda = 10^{-4}$ are practically indistinguishable. Finally, the 3D, 4D and 7D integrals (depending on the trial helium functions) are calculated numerically using the Fortran code Cuhre [39].

PWSBA and the closure approximation

We use the abbreviation PWSBA to emphasize that the proton is described by the plane wave. It follows from (4) if in the expansion of the final-state wave function in powers of $1/v_p$ and $1/|\vec{v}_p - \vec{k}_e|$ we retain only the zeroth- and first-order terms:

$$\mathcal{T}(\vec{v}_p, \vec{Q}, \vec{k}_e) = T^{PWFBA}(\vec{Q}, \vec{k}_e) + T^{PWSBA}(\vec{v}_p, \vec{Q}, \vec{k}_e). \tag{12}$$

The PWSBA term is given by

$$T_{fi}^{\text{PWSBA}} = \frac{2\sqrt{2}}{\pi} \sum_\alpha \int \frac{d^3x}{x^2(\vec{Q} - \vec{x})^2[\vec{v}_p \cdot \vec{x} + \varepsilon_0^{He} - \varepsilon_\alpha^{He} + i0]}$$
$$\times \int d^3r_1 d^3r_2 \Phi_f^{He(-*)}(\vec{r}_1, \vec{r}_2; \vec{k}_e) \left[2 - e^{i(\vec{Q}-\vec{x})\vec{r}_1} - e^{i(\vec{Q}-\vec{x})\vec{r}_2} \right] \Phi_\alpha^{He(-)}(\vec{r}_1, \vec{r}_2)$$
$$\times \int d^3r'_1 d^3r'_2 \Phi_\alpha^{He(-*)}(\vec{r}'_1, \vec{r}'_2) \left[2 - e^{i\vec{x}\vec{r}'_1} - e^{i\vec{x}\vec{r}'_2} \right] \Phi_0^{He}(\vec{r}'_1, \vec{r}'_2). \tag{13}$$

The sum in Eq. (13) runs over all helium eigenstates including single and double continuum.

Since the proton velocity is large, we use the closure approximation $\varepsilon_\alpha^{He} - \varepsilon_0^{He} \to \bar{E} > 0$. In this case we get

$$T_{fi}^{\text{PWSBA}} = \frac{2\sqrt{2}}{\pi} \int \frac{d^3x}{x^2(\vec{Q} - \vec{x})^2[\vec{v}_0 \cdot \vec{x} - \bar{E} + i0]}$$
$$\times \int d^3r_1 d^3r_2 \Phi_f^{He(-*)}(\vec{r}_1, \vec{r}_2; \vec{k}_e)[2 - e^{i(\vec{Q}-\vec{x})\vec{r}_1} - e^{i(\vec{Q}-\vec{x})\vec{r}_2}][2 - e^{i\vec{x}\vec{r}_1} - e^{i\vec{x}\vec{r}_2}]\Phi_0^{He}(\vec{r}_1, \vec{r}_2). \tag{14}$$

For the initial state we use the Hylleraas wave function (the ground-state energy is $\varepsilon_0^{Hy} = -0.2862$ a.u.)

$$\Phi_0^{He}(\vec{r}_1, \vec{r}_2) = \phi(r_1)\phi(r_2), \qquad \phi(r) = \sqrt{\frac{Z_h^3}{\pi}}e^{-Z_h r}, \qquad Z_h = 27/16. \tag{15}$$

The final single-electron state is taken in the simplest form

$$\Phi_f^{He(-*)}(\vec{r}_1, \vec{r}_2; \vec{k}_e) = \tilde{\phi}^{-*}(\vec{k}_e, \vec{r}_1; -1)\varphi^{He^+}(r_2).$$

Our formulation of PWSBA is very close to that in the work [7]. It is interesting to note that numerically and theoretically the PWSBA results using the closure approximation are very similar to those obtained within the eikonal wave Born approximation (EWBA). Earlier this particular approach was formulated in Ref. [40]. It was noted that all the interactions involved in the perturbation contribute to the corresponding matrix element on an equal footing, that is, not only the projectile-nucleus interaction appears to be important.
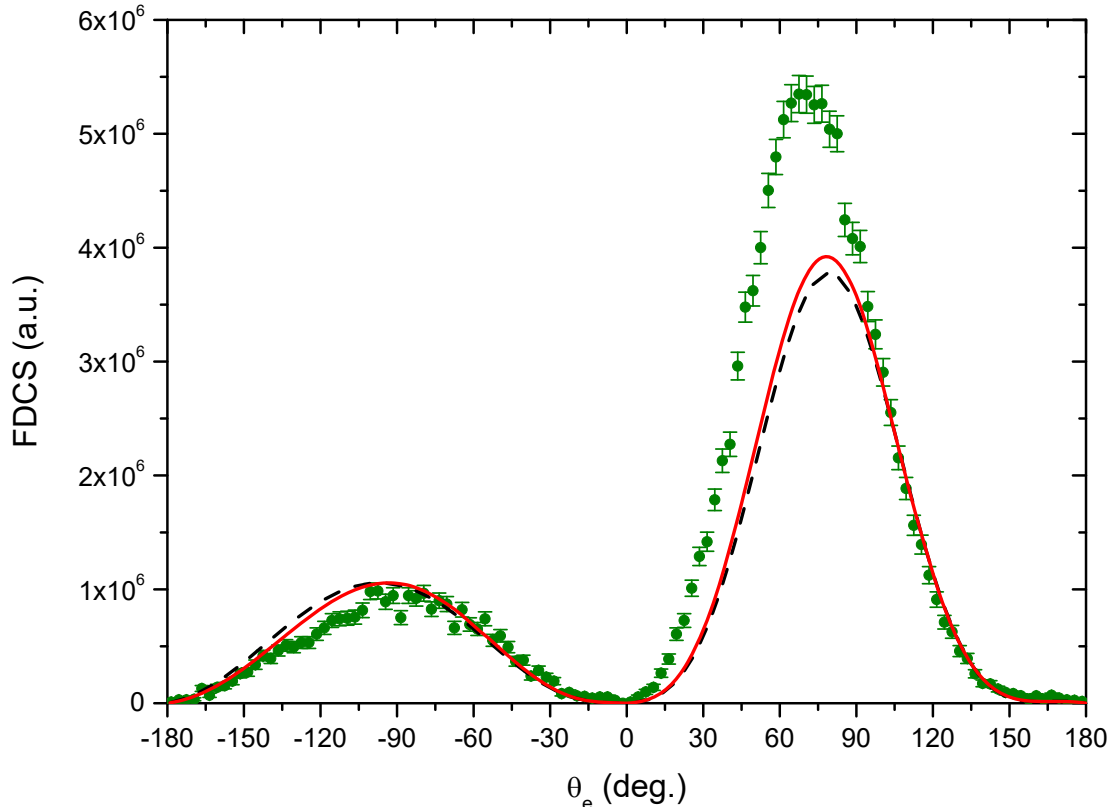
FIG. 1.   (Color online) FDCS in coplanar geometry using the PWFBA (black dashed line) and PWSBA (red solid line) with the Hy ground state of the He atom (15). Experimental values are represented by points, $\lambda = 10^{-3}$, $\bar{E} = 0.9$.

III.   RESULTS AND DISCUSSION

In this section we present results of numerical calculations for FDCS as a function of the electron scattering angle θ_e in the coplanar geometry, which were obtained using the theoretical approaches outlined in the previous section. For comparison with experiment, the theoretical results were convoluted with an angular resolution of $5°$, both in polar and in azimuthal angles, and averaged over the out-of-plane electron angle $\phi_e = 0 \pm 10°$ (see details in the Appendix A). As the experiment was performed on an arbitrary intensity scale, the experimental values were normalized to the convoluted and averaged FDCS in the case of the 3C model (5) and the CF ground-state function of He.

The electron angular distribution within PWFBA typically exhibits two distinct peaks of larger and smaller intensity respectively: the binary peak in the direction of momentum transfer and the recoil peak in the opposite direction. In our previous calculations [16], it was
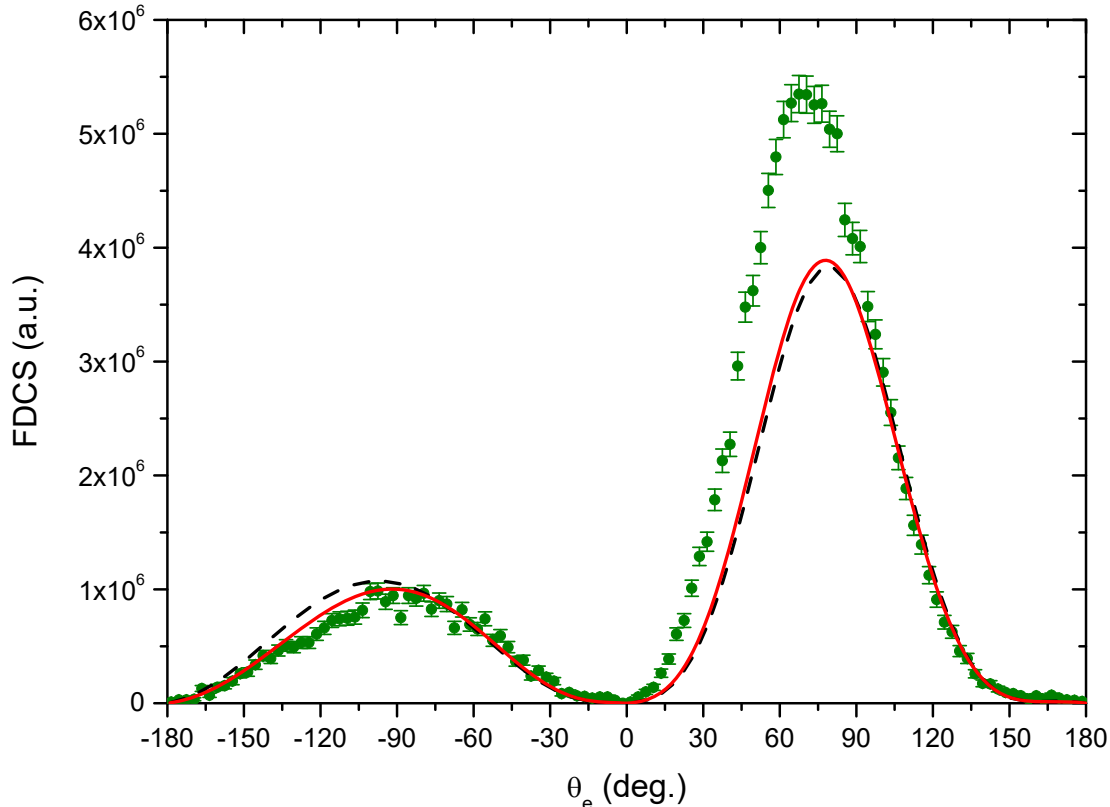
FIG. 2. (Color online) FDCS in coplanar geometry using the PWFBA (black dashed line) and 3C model (red solid line) with the RHF ground state of the He atom. Experimental values are represented by points, $\lambda = 10^{-3}$.

found that the measured binary and recoil peaks in coplanar geometry are shifted by almost 10° towards the incident proton direction with respect to the PWFBA theory. This is an unambiguous signature of the collision mechanisms beyond PWFBA. In Fig. 1, the PWFBA results using the Hy function (15) are presented along with the PWSBA calculations and experimental values. The PWFBA and PWSBA cross sections appear to be close to each other. At the same time, the binary and recoil peaks in the PWSBA case are shifted (by $\sim$3°-5°) relative to the PWFBA ones towards the $\theta_e = 0°$ direction. Displacement of the binary peak practically is not changed within wide domain $0.1 \lesssim \bar{E} \lesssim 1.7$, and is too small for explaining positions of the peaks' maximums in the experimental angular distribution, indicating that the higher-order effects, beyond PWSBA, should be taken into account.

As remarked in the previous section, PWFBA and PWSBA follow from the 3C model upon expansion in powers of $1/v_p$ and $1/|\vec{v}_p - \vec{k}_e|$. In other words, the 3C model effectively
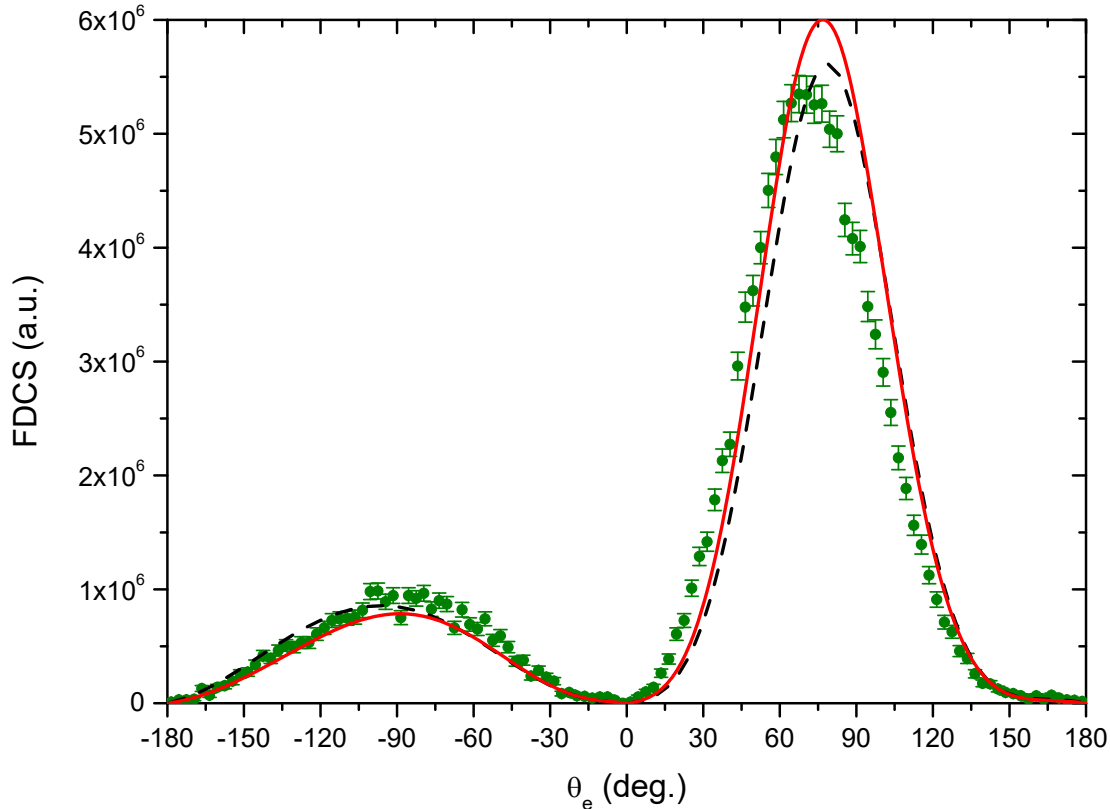
FIG. 3. (Color online) The same as in Fig. 2, but in the case of the SPM ground state of the He atom.

includes higher-order collision mechanisms unaccounted by these approximations. Figure 2 shows the PWFBA and 3C results in the case of the RHF function in comparison with experiment. The difference between the PWFBA and 3C results is not very significant. Similar to PWSBA, the 3C model provides the shift of both PWFBA peaks towards the experiment. The shift for the binary peak is much smaller than for the recoil peak and is not enough to explain the experiment. It is clear that the ratio of measured peak intensities (recoil/binary) does not depend on the employed normalization of experiment. In this respect, both the PWFBA and the 3C results substantially disagree with experiment. This disagreement is due to a poor account for electron-electron correlations in the He ground state with the RHF model. The effect of electron-electron correlations in He is known to be strong and cannot be appropriately treated by mean-field approaches such as RHF. Even the simple SPM function of the configuration interaction family describes this effect much better. As can be seen from Fig. 3, it gives the value of the recoil/binary ratio which is
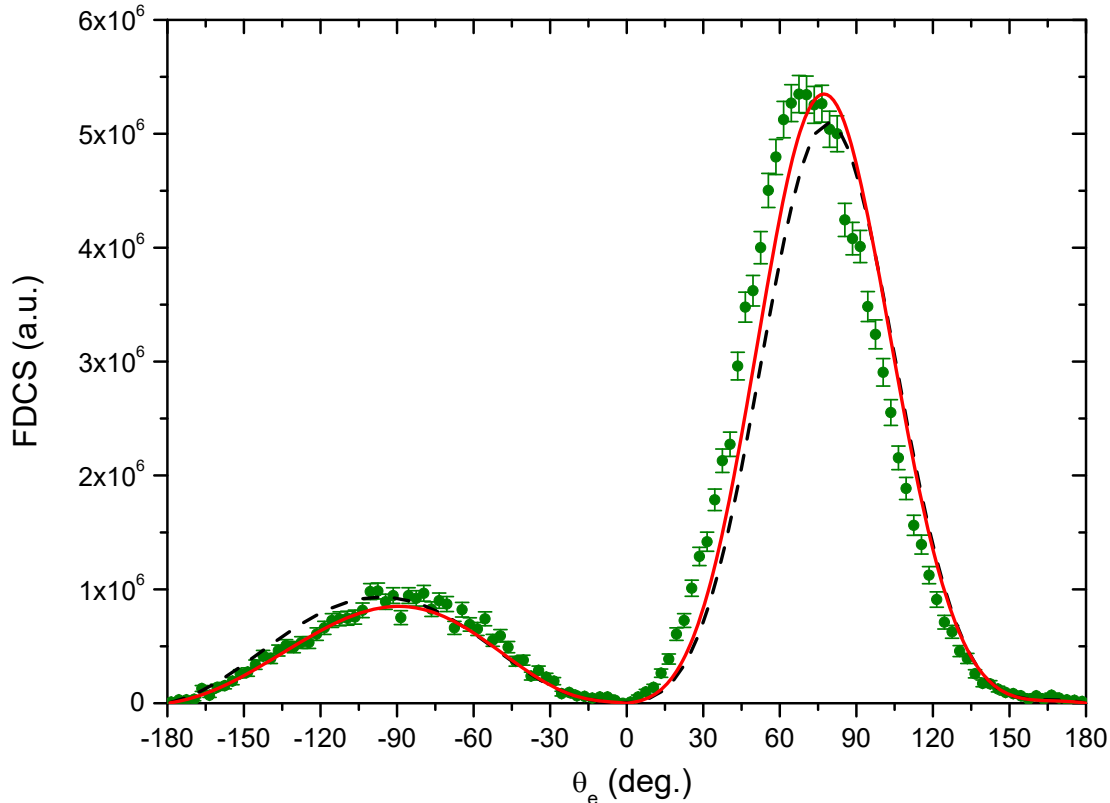
FIG. 4. (Color online) The same as in Fig. 2, but in the case of the CF ground state of the He atom.

notably closer to the experiment than in the RHF case. The differences between the PWFBA and 3C results using the SPM function are similar to those in Fig. 2.

Figure 4 compares with experiment the PWFBA and 3C calculations using the CF function. The 3C model gives good agreement with experiment in terms of the recoil/binary ratio and differs from the PWFBA results in a similar way as in Figs. 2 and 3.

We compared our in-plane results without convolution with those reported recently in Ref. [21] (see Fig. 1 therein). For making the comparison, we multiplied the scale employed in Ref. [21] by the factor $k_e p_i^2$. Our 3C results using the CF function fully agree with those in Ref. [21]. This finding is surprising because we would expect an agreement with our results using the RHF function rather than the CF function. Indeed, the author of Ref. [21] calculated the helium ground-state function using a simple one-electron radial potential and neglecting the correlation between electrons in helium. At the same time, the shift of the binary peak in Ref. [21] is the same as in the present paper, i.e. it is not sufficient to explain

the experimental binary-peak position.

In order to inspect which final-state interaction is mainly responsible for the shift of the binary and recoil peaks, we performed the 3C calculations with the CF function in the following situations: (i) $1/v_p = 0$, i.e. no proton-ion interaction in the final state, and (ii) $1/|\vec{v}_p - \vec{k}_e| = 0$, i.e. no proton-electron interaction in the final state. The results of such test calculations are shown in Fig. 5. One would expect that the shift of the peaks is due to the proton-electron rather than the proton-ion interaction, since the proton, after knocking-out the electron from the atom, attracts the electron and thus should distort the outgoing electron trajectory in the forward direction. The results presented in Fig. 5 agree with this expectation concerning the recoil peak but contradict it regarding the binary peak. It turns out that it is the proton-ion interaction that is responsible for the shift of the binary peak towards smaller θ_e values, while the proton-electron interaction shifts the binary peak in the opposite direction. Moreover, the shift in the $1/v_p = 0$ case is large enough to explain the position of the binary peak in experiment. It is worth mentioning that the conclusion that for small momentum transfers it is the proton-nucleus interaction that mostly leads to a shift of the binary peak has been formulated earlier in Ref. [41].

IV. SUMMARY AND CONCLUSIONS

Theoretical calculations beyond the PWFBA theory have been presented and compared with experiment in coplanar geometry. The roles of higher-order collision mechanisms have been examined using the PWSBA and 3C approaches. Three different ground-state wave functions of He have been employed in the calculations. It has been shown that for explaining the recoil peak/binary peak ratio it is necessary to account for the strong effect of electron-electron correlations in the ground state of the He atom. The PWSBA treatment has been found to be insufficient for describing the shift of the binary and recoil peaks in the electron angular distribution with respect to the PWFBA prediction. In this respect, the 3C model reasonably agrees with experiment in the recoil peak, but a discrepancy of few degrees with experiment still remains in the case of the binary peak. Our test calculations within the 3C model have yielded a counter-intuitive result, namely that the shift of the binary peak towards smaller electron angles is due to the proton-ion interaction in the final state. This finding contradicts a naive expectation that this shift is due to the proton-electron interaction
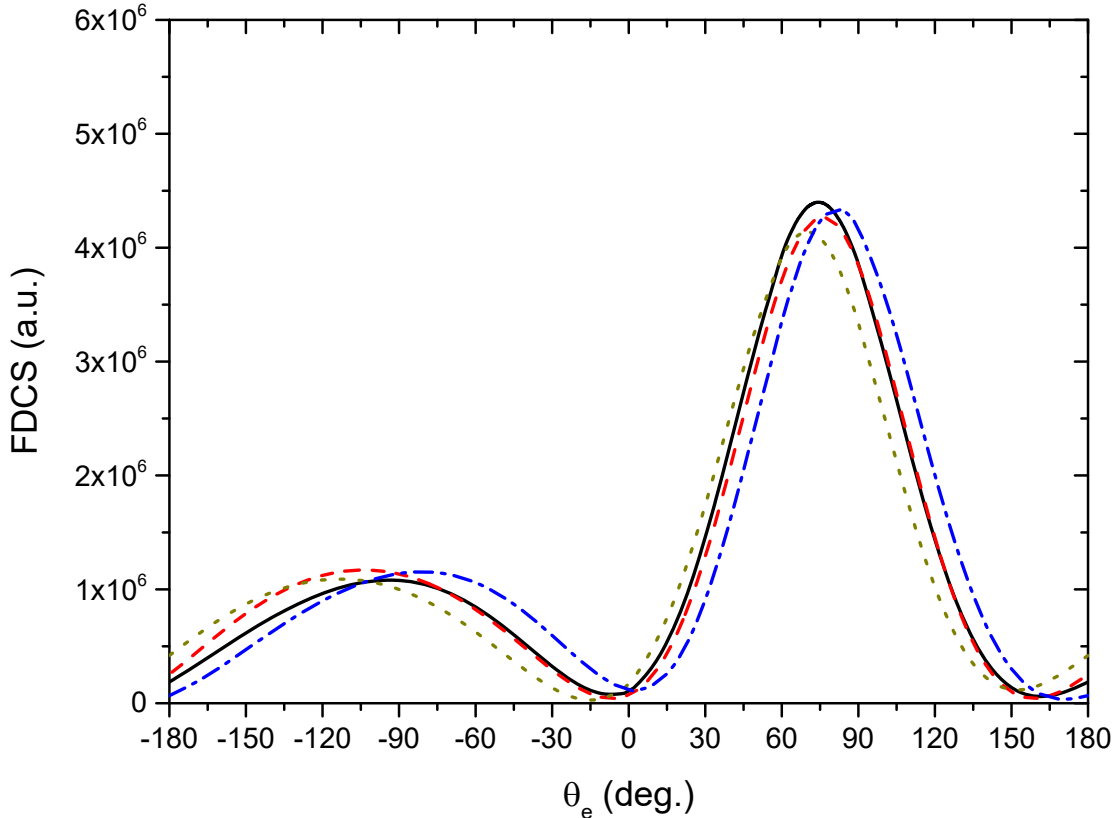
14

FIG. 5. (Color online) FDCS in the case of the CF ground state of the He atom within PWFBA (red dashed line), 3C model (black solid line), and the 3C model with $1/v_p = 0$ (blue dash-dotted line) and $1/|\vec{v}_p - \vec{k}_e| = 0$ (bronze yellow dotted line). $\lambda = 10^{-3}$.

in the final state. Surprisingly, the latter interaction shifts the binary peak in the opposite direction. Thus, further theoretical studies are needed to explain the discrepancy between theory and experiment in coplanar geometry.

ACKNOWLEDGMENTS

from the Hulubei-Meshcheryakov program JINR-Romania. A. G. is "aspirant au Fonds de la Recherche Scientifique (F.R.S-FNRS)"

Appendix A: Convolution of theoretical values with experimental uncertainties

Let the 2D cross section $\sigma^{2D}(\theta, \phi)$ to be tabulated in the points (θ_i, ϕ_j), $i = 1, \ldots, M$, $j = 1, \ldots, N$. In the convolution procedure, we use the following Gaussian function at each point (θ_i, ϕ_j):

$$G^{2D}(\theta, \phi, \theta_i, \phi_j) = \frac{1}{w_\theta \sqrt{2\pi}} \frac{1}{w_\phi \sqrt{2\pi}} \exp\left(-\frac{1}{2}\left(\frac{\theta - \theta_i}{w_\theta}\right)^2 - \frac{1}{2}\left(\frac{\phi - \phi_j}{w_\phi}\right)^2\right) \quad \text{(A1)}$$

with full width at half maximum (FWHM)

$$\text{FWHM} = 2\sqrt{2\ln(2)}\, w_\theta = 2\sqrt{2\ln(2)}\, w_\phi. \quad \text{(A2)}$$

The convoluted discrete FDCS, $\sigma_C^{2D}(\theta, \phi)$, is constructed at the given point (θ_i, ϕ_j) according to

$$\sigma_C^{2D}(\theta_i, \phi_j) = \sum_{k=\max(-K,1-i)}^{\min(K,M-i)} \sum_{l=\max(-L,1-j)}^{\min(L,N-j)} G^{2D}(\theta_i, \phi_j, \theta_{i+k}, \phi_{j+l}) \sigma^{2D}(\theta_{i+k}, \phi_{j+l}). \quad \text{(A3)}$$

Here

$$K = [\text{FWHM}/h_\theta] + 1, \qquad L = [\text{FWHM}/h_\phi] + 1, \quad \text{(A4)}$$

where h_θ and h_ϕ are steps of the θ and ϕ angles, and $[x]$ denotes an integer part of x.

In the present case, we used $M = 361$, $N = 21$, $h_\theta = h_\phi = 1°$, $\theta_i = (i-1)h_\theta$, $\phi_j = -10° + (i-1)h_\phi$ and FWHM= 5. The convoluted FDCS are further averaged over angular windows, so that one has for coplanar geometry

$$\sigma_C^{1D}(\theta, \phi = 0°) = |\sin(\theta)| \int_{-10°}^{10°} d\phi' \sigma_C^{2D}(\theta, \phi'). \quad \text{(A5)}$$

The integral in (A5) is calculated numerically using points ϕ_j, $j = 1, \ldots, N$ for given $\theta = \theta_i$, $i = 1, \ldots, M$.

---

[1] J. Ullrich, R. Moshammer, R. Dörner, O. Jagutzki, V. Mergel, H. Schmidt-Böcking, and L. Spielberger, J. Phys. B **30**, 2917 (1997).

[2] R. Dörner, V. Mergel, O. Jagutzki, L. Spielberger, J. Ullrich, R. Moshammer, and H. Schmidt-Böcking, Phys. Rep. **330**, 95 (2000).

[3] J. Ullrich, R. Moshammer, A. Dorn, R. Dörner, L. Ph. H. Schmidt, and H. Schmidt-Böcking, Rep. Prog. Phys. **66**, 1463 (2003).

[4] M. Schulz, R. Moshammer, D. Fischer, H. Kollmus, D. H. Madison, S. Jones, and J. Ullrich, Nature **422**, 48 (2003).

[5] D. Madison, M. Schulz, S. Jones, M. Foster, R. Moshammer, and J. Ullrich, J. Phys. B **35**, 3297 (2002).

[6] A. B. Voitkiv, B. Najjari, and J. Ullrich, J. Phys. B: At. Mol. Opt. Phys. **36**, 2591 (2003).

[7] M. McGovern, C. T. Whelan, and H. R. J. Walters, Phys. Rev. A **82**, 032702 (2010).

[8] K. A. Kouzakov, S. A. Zaytsev, Yu. V. Popov, and M. Takahashi, Phys. Rev. A **86**, 032710 (2012).

[9] M. F. Ciappina and W. R. Cravero, J. Phys. B: At. Mol. Opt. Phys. **39**, 1091 (2006).

[10] A. L. Harris, D. H. Madison, J. L. Peacher, M. Foster, K. Bartschat, and H. P. Saha, Phys. Rev. A **75**, 032718 (2007).

[11] M. McGovern, D. Assafrão, J. R. Mohallem, C. T. Whelan, and H. R. J. Walters, Phys. Rev. A **81**, 042704 (2010).

[12] J. Colgan, M. S. Pindzola, F. Robicheaux, and M. F. Ciappina, J. Phys. B: At. Mol. Opt. Phys. **44**, 175205 (2011).

[13] J. Fiol, S. Otranto, and R. E. Olson, J. Phys. B **39**, L285 (2006).

[14] X. Wang, K. Schneider, A. LaForge, A. Kelkar, M. Grieser, R. Moshammer, J. Ullrich, M. Schulz, D. Fischer, J. Phys. B: At. Mol. Opt. Phys. **45**, 211001 (2012).

[15] M. Durr, B. Najjari, M. Schulz, A. Dorn, R. Moshammer, A. B. Voitkiv, and J. Ullrich, Phys. Rev. A **75**, 062708 (2007).

[16] H. Gassert, O. Chuluunbaatar, M. Waitz, F. Trinter, H.-K. Kim, T. Bauer, A. Laucke, Ch. Müller, J. Voigtsberger, M. Weller, J. Rist, M. Pitzer, S. Zeller, T. Jahnke, L. Ph. H. Schmidt, J.B. Williams, S.A. Zaytsev, A. A. Bulychev, K. A. Kouzakov, H. Schmidt-Böcking, R. Dörner, Yu.V. Popov, M.S. Schöffler, Phys. Rev. Lett. **116**, 073201 (2016).

[17] T. Arthanayaka, B. R. Lamichhane, A. Hasan, S. Gurung, J. Remolina, S. Borbély, F. Járai-Szabó, L. Nagy, and M. Schulz, J. Phys. B: At. Mol. Opt. Phys. **49**, 13LT02 (2016).

[18] K. A. Kouzakov, Eur. Phys. J. D **71**, 63 (2017).

[19] F. Navarrete, M. F. Ciappina, L. Sarkadi, and R. O. Barrachina, Nucl. Instrum. and Meth. B **408**, 165 (2017).

[20] L. Nagy, Sándor Borbély, and F. Járai-Szabó, J. Phys.: Conf. Ser. **875**, 092009 (2017).

[21] A.B. Voitkiv, Phys. Rev. A **95**, 032708 (2017).

[22] H. R. Dodd, K. R. Greider. Phys. Rev. **146**, 675 (1966).

[23] R. Gayet, J. Phys. B: At. Mol. Phys. **5**, 483 (1972).

[24] G. Gasaneo, W. Cravero, M. D. Sanchez, and C. R. Garibotti, Phys. Rev A **54**, 439 (1996).

[25] J. M. Cheshire, Proc. Phys. Soc. **84**, 89 (1964).

[26] D. S. F. Crothers, J. Phys. B: At. Mol. Phys. **15**, 2061 (1982).

[27] D. S. F. Crothers and J. F. McCann, J. Phys. B: At. Mol. Phys. **16**, 3229 (1983).

[28] M. F. Ciappina, O. A. Fojon, and R. D. Rivarola, J. Phys. B: At. Mol. Opt. Phys. **47**, 042001 (2014).

[29] J. M. Monti, O. A. Fojon, J. Hanssen, and R. D. Rivarola, J. Phys. B: At. Mol. Opt. Phys. **46**, 145201 (2013); *ibid.* **42**, 195201 (2009).

[30] Dz. Belkic, R. Gayet, and A. Salin, Phys. Rep. **56**, 281 (1979).

[31] D. S. F. Crothers and L. J. Dube, Adv. At. Mol. Opt. Phys. **30**, 287 (1993).

[32] M. Brauner, J. S. Briggs, and H. Klar, J. Phys. B: At. Mol. Opt. Phys. **22**, 2265 (1989).

[33] A. Mondal, Ch. Mandal, and M. Purkait, Eur. Phys. J. D **70**, 16 (2016).

[34] J. Dollard, J. Math. Phys. **5**, 729 (1964).

[35] E. Clementi and C. Roetti, At. Data Nucl. Data Tables **14**, 177 (1974).

[36] J. N. Silvermann, O. Platas, and F. A. Matsen, J. Chem. Phys. **32**, 1402 (1960).

[37] O. Chuluunbaatar, I. V. Puzynin, P. S. Vinitsky, Yu. V. Popov, K. A. Kouzakov, and C. Dal Cappello, Phys. Rev. A **74**, 014703 (2006).

[38] L. D. Landau and E. M. Lifshitz, *Quantum mechanics: non-relativistic theory, 3rd edition*, (Pergamon Press, 1977), §150.

[39] http://www.feynarts.de/cuba/

[40] Hong-Keun Kim, M. S. Schöffler, S. Houamer, O. Chuluunbaatar, J. N. Titze, L. Ph. H. Schmidt, T. Jahnke, H. Schmidt-Boecking, A. Galstyan, Yu. V. Popov, and R. Dörner. Phys. Rev. A. **85**, 022707 (2012).

[41] M. Schulz, B. Najjari, A. B. Voitkiv, K. Schneider, X. Wang, A. C. Laforge, R. Hubele, J. Goullon, N. Ferreira, A. Kelkar, M. Grieser, R. Moshammer, J. Ullrich, and D. Fischer. Phys.

Rev. A. **88**, 022704 (2013)